Article:

Kunert, A., Poulton, S.W. orcid.org/0000-0001-7621-189X, Canfield, D.E. et al. (3 more authors) (Accepted: 2025) Controls on uranium isotope fractionation in the Late Paleoproterozoic ocean. Earth and Planetary Science Letters. ISSN 0012-821X (In Press)

Supplement for

Controls on uranium isotope fractionation in the Late Paleoproterozoic ocean

Animikie Basin Tectonic Setting

Early studies interpreted the Animikie Basin as a foreland assemblage with load-driven subsidence resulting from Penokean Orogeny thrusting in the south (Barovich et al., 1989; Hoffman, 1987; Klasner et al., 1991; Morey and Southwick, 1995; Ojakangas et al., 2001; Southwick and Morey, 1991). However, studies of Nd and common Pb (Hemming et al., 1995), Sm–Nd and U–Pb (Van Wyck and Johnson, 1997) and U–Pb geochronology (Fralick et al., 2002) have indicated that the foreland model is not applicable to the basin where the Gunflint and Biwabik iron formations were deposited. Additionally, the Gunflint and Biwabik iron formations are at least ~10 million years older than commencement of Penokean deformation (Fralick et al., 2002), and they contain very little siliciclastic sediment (Larson, 2013), incompatible with a mountainous terrain to the immediate south. Large areas of Penokean deformation have been reinterpreted as Yavapai (Holm et al., 2018, 2005), and geochronology of the area fringing the Superior Craton indicates an extensional regime at 1.88 Ga (Bleeker et al., 2019). The siliciclastics of the Rove and Virginia formations appear to have been deposited in a peripheral foreland setting on the edge of the craton, but with subsidence due to tectonic loading during the 1.83 Ga Trans-Hudson Orogeny. This is indicated by pro-delta outbuilding from the direction of the Trans-Hudson Orogenic zone to the northwest (Johnston et al., 2006; Maric and Fralick, 2005) and paleocurrents indicating sediment delivery from that direction (Morey, 1969, 1967).

GF-3 Additional Digestion

The GF-3 core samples were not fully dissolved following the total digestion procedure outlined in the main text. The following additional steps were taken to dissolve these samples. *Aqua regia* and HCl digestions were repeated, followed by 9 mL inverse *aqua regia* (2:1 HNO_3/HCl) at 150°C for 48 hours. These samples still featured residual and supernatant phases, so the supernatant was pipetted and both phases were further digested by inverse *aqua regia* and concentrated HCl. Three types of visible solids were still present: a greasy film (surface), clumped particles that dissolved when slurried, and disseminated fine-grained particles. A final attempt to dissolve these residues in 1:1 HNO_3 and 30% hydrogen peroxide (H_2O_2) resulted in all residues becoming disseminated or fully dissolved. Supernatant and residual phases were dried and redissolved in 6 M HCl, then reintegrated. Procedural blanks produced with these samples were comparable to other batches.

Macroscopic Pyrite in Core 89-MC-1

Macroscopic (up to 1 mm) pyrite layers and disseminated clusters (Figure S1) occur in the 'dynamic interval' of core 89-MC-1 (86.000–86.303 m above Gunflint Fm.). The laminated morphology and occurrence during the transition from a ferruginous to euxinic water column suggests intense sulfide production at the sediment water interface, likely with sulfide diffusing into the water column, thereby resulting in large scale drawdown of Fe^{2+} from the water column. This is also supported by a relatively homogeneous pyrite sulfur isotope composition for this interval ($\delta^{34}S$ = 9.99–12.45‰), suggesting a constant, well-mixed sulfate/sulfide source, most likely of water-column origin (Poulton et al., 2004) .

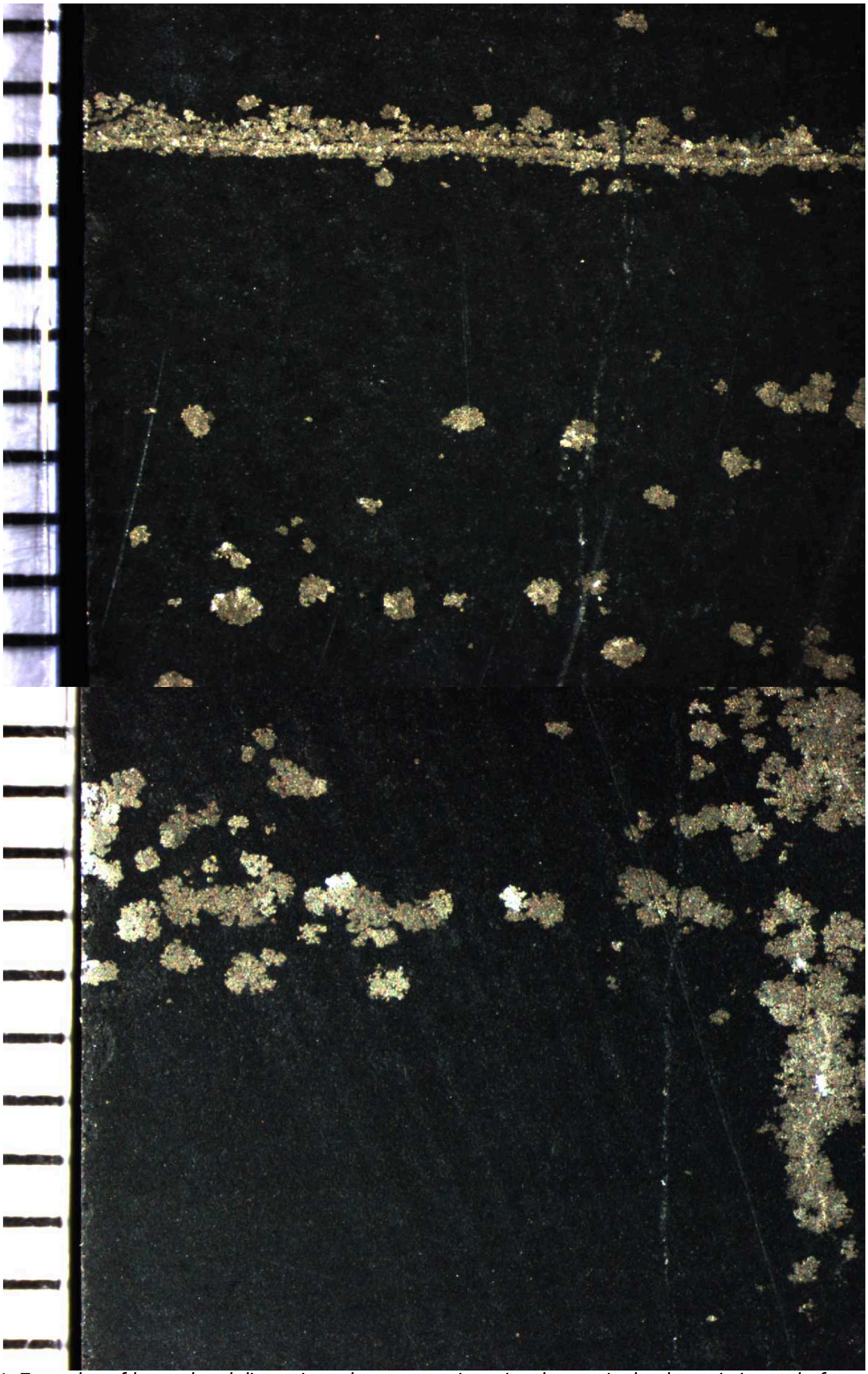

Figure S1. Examples of layered and disseminated macroscopic pyrite clusters in the dynamic interval of core 89-MC-1 (86.000 – 86.303 m above Gunflint Fm). Scale bar is in millimeters.

Modified Proterozoic Two-sink δ^{238}U Mass Balance

Application of a modified two-sink steady state mass balance (Eq. S1; after Gilleaudeau et al., 2019; Wang et al., 2016; Yang et al., 2017) shows how modern-like $\delta^{238}U_{sw}$ can occur in an anoxic Proterozoic ocean, and how lower $\delta^{238}U_{sw}$ (−0.73‰) can be achieved with increased primary productivity on continental margins:

$$\text{(S1)} \qquad \delta^{238}\mathrm{U}_{\mathrm{sw}} = \delta^{238}\mathrm{U}_{\mathrm{riv}} - \frac{\left(\sum k_i A_i \Delta^{238}\mathrm{U}_{i-\mathrm{sw}}\right)}{\sum k_i A_i}$$

where *i* is a given U sediment sink, k_i is an areal burial rate factor for a sink, and A_i is the seafloor area of a sink. The $\delta^{238}U_{riv}$ value is set to the modern value (−0.29‰). Using the Animikie Basin data, we define two sinks where (1) large isotopic fractionations from 0.4‰ to 1.2‰ are observed in environments with higher primary productivity associated with the euxinic wedge and adjacent locations (TOC = 2.3 ± 0.9 wt%, signified with a subscript *h* for higher TOC), and (2) smaller isotopic fractionations from −0.1‰ to 0.4‰ in areas with lower primary productivity associated with low-oxygen or deep ferruginous settings (TOC = 0.8 ± 0.7 wt%, signified with a subscript *l* for lower TOC). Equation 1 is rearranged assuming $A_l = 1 - A_h$ to solve for A_h (Eq. S2):

$$\text{(S2)} \qquad A_h = \frac{\left(k_l\left(\Delta^{238}\mathrm{U}_{l-\mathrm{sw}} - \delta^{238}\mathrm{U}_{\mathrm{riv}} + \delta^{238}\mathrm{U}_{\mathrm{sw}}\right)\right)}{k_h\left(\delta^{238}\mathrm{U}_{\mathrm{riv}} - \delta^{238}\mathrm{U}_{\mathrm{sw}} - \Delta^{238}\mathrm{U}_{h-\mathrm{sw}}\right) + k_l\left(\Delta^{238}\mathrm{U}_{l-\mathrm{sw}} - \delta^{238}\mathrm{U}_{\mathrm{riv}} + \delta^{238}\mathrm{U}_{\mathrm{sw}}\right)}$$

Scaling factors (k_i) are based on modern burial rate data, where k_{oxic} is 0.048 dm yr^{-1}, k_{anoxic} is 0.469 dm yr^{-1}, and $k_{euxinic}$ is 2.534 dm yr^{-1} (Gilleaudeau et al., 2019; Wang et al., 2016; Yang et al., 2017). In our model, it is unlikely that k_{oxic} is representative of burial rates in the low TOC sink as U enrichment ($U_{EF} > 1$) is still recorded and has been shown to scale with U accumulation rate (Clarkson et al., 2023), although sedimentary U burial rates likely decreased with distance from the paleoshoreline. Therefore, we apply a range between k_{oxic} and k_{anoxic} of 0.048–0.469 dm yr^{-1} for k_l, and a range from k_{anoxic} to $k_{euxinic}$ of 0.469–2.534 dm yr^{-1} for k_h. The model was built in Python (v3.9) and varied each parameter from minimum to maximum values in 10 steps (Table 2). Modelling results are presented in Table S1 and outputs are shown in Figs. S2, S3 and S4.

Table S1. *Uranium isotope mass balance model parameters. Subscript 'l' denotes low TOC sink, subscript 'h' denotes high TOC sink.*

Parameter	Unit	Minimum	Maximum	Step Size
k_l	dm yr^{-1}	0.048	0.469	0.0421
k_h		0.469	2.534	0.2065
$\delta^{238}U_{sw}$*	‰	−0.73	−0.29	0.044
$\delta^{238}U_{riv}$		−0.29 (constant)		
$\Delta^{238}U_{l\text{-}sw}$		−0.1	0.4	0.05
$\Delta^{238}U_{h\text{-}sw}$		0.4	1.2	0.08

* Cases with $\delta^{238}U_{sw}$ set to mid-Proterozoic mean, −0.40‰, and minimum, −0.73‰, were also modelled.

Table S2. *Uranium isotope mass balance model results for area of highly productive seafloor (A_h) for selected model scenarios.*

Scenario	Median A_h (%$_{total\ seafloor}$)	1st Quartile A_h	3rd Quartile A_h
Total model parameter ranges	5.0	1.8	12.4
$\delta^{238}U_{sw}$ set to −0.40‰	2.1	0.7	4.7
$\delta^{238}U_{sw}$ set to −0.73‰	10.3	4.3	22.5

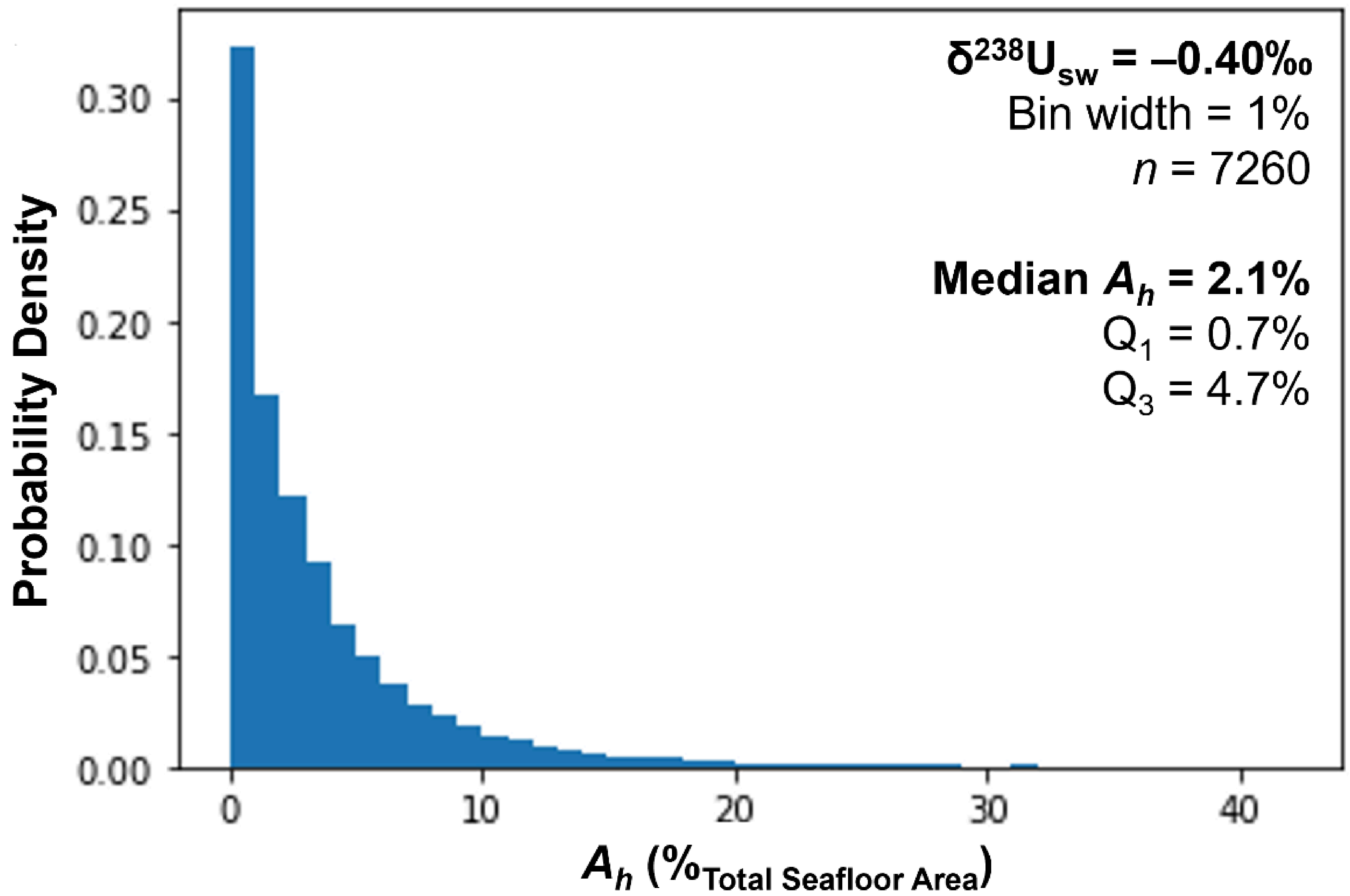

Figure S2. Uranium mass balance model output for a scenario with modern-like $\delta^{238}U_{sw}$ as estimated for the average Proterozoic oceans by Chen et al. (2021). A_h = area of highly productive seafloor.

These results align with a previous $\delta^{238}U$ model suggesting limited areas of euxinia in the Proterozoic ocean (likely < ~10% total seafloor; Gilleaudeau et al., 2019). However, unlike the previous estimate, we do not limit large U isotope fractionations to the euxinic seafloor. Areas with a large sinking TOC flux are prone to development of euxinia, but euxinia is not a prerequisite. This contrasts with the sediment sink receiving limited TOC, which in the shallower settings results in low-oxygen conditions where U may have been only mildly reduced, deeper-water locations where an abundance of Fe^{2+} could have rapidly reduced U, or in either location where U may have adsorbed to solid Fe/Mn species. These scenarios impart minimal or potentially small negative isotopic fractionations, thus producing the isotopically light $\delta^{238}U_{sw}$ in such samples. Together, these settings make up the remainder of the seafloor beyond A_h (A_l = 90.1–98.1% of the total Proterozoic seafloor given $\delta^{238}U_{sw}$ from modern-like to minimum Proterozoic estimates).

Model Code

The code for the mass balance model (Equation 2) was built in Python v3.9 and is pasted in the section below. The first block can be used to estimate the global area of high productivity (A_h) for a specific $\delta^{238}U_{sw}$ (set to –0.73‰ below). Results depicted in main text Figure 8 (modern seawater) and Figure S2 (minimum Proterozoic estimate).

```
import matplotlib as plt
import numpy as np

#Article Equation 5

def A_high(k_low,k_high,D_low,D_high,d_sw):
    d_riv = -0.29
    num = k_low * (D_low - d_riv + d_sw)
    denom = k_high*(d_riv - d_sw - D_high) + num
    return num/denom * 100

#Seawater Estimate (permil)

d_sw = -0.73

#Produce A_high histogram for selected seawater estimate (d_sw)

Areas = []
for k_l in np.arange(0.048,0.5111,0.0421):
    for k_h in np.arange(0.469,2.7405,0.2065):
        for D_l in np.arange(-0.1,0.45,0.05):
            for D_h in np.arange(0.4,1.28,0.08):
                A = A_high(k_l,k_h,D_l,D_h,d_sw)
                if 0 <= A <= 100:
                        Areas.append(A)

plt.pyplot.hist(Areas,100,None,True)
print(np.percentile(Areas,(25,50,75)),len(Areas))
```

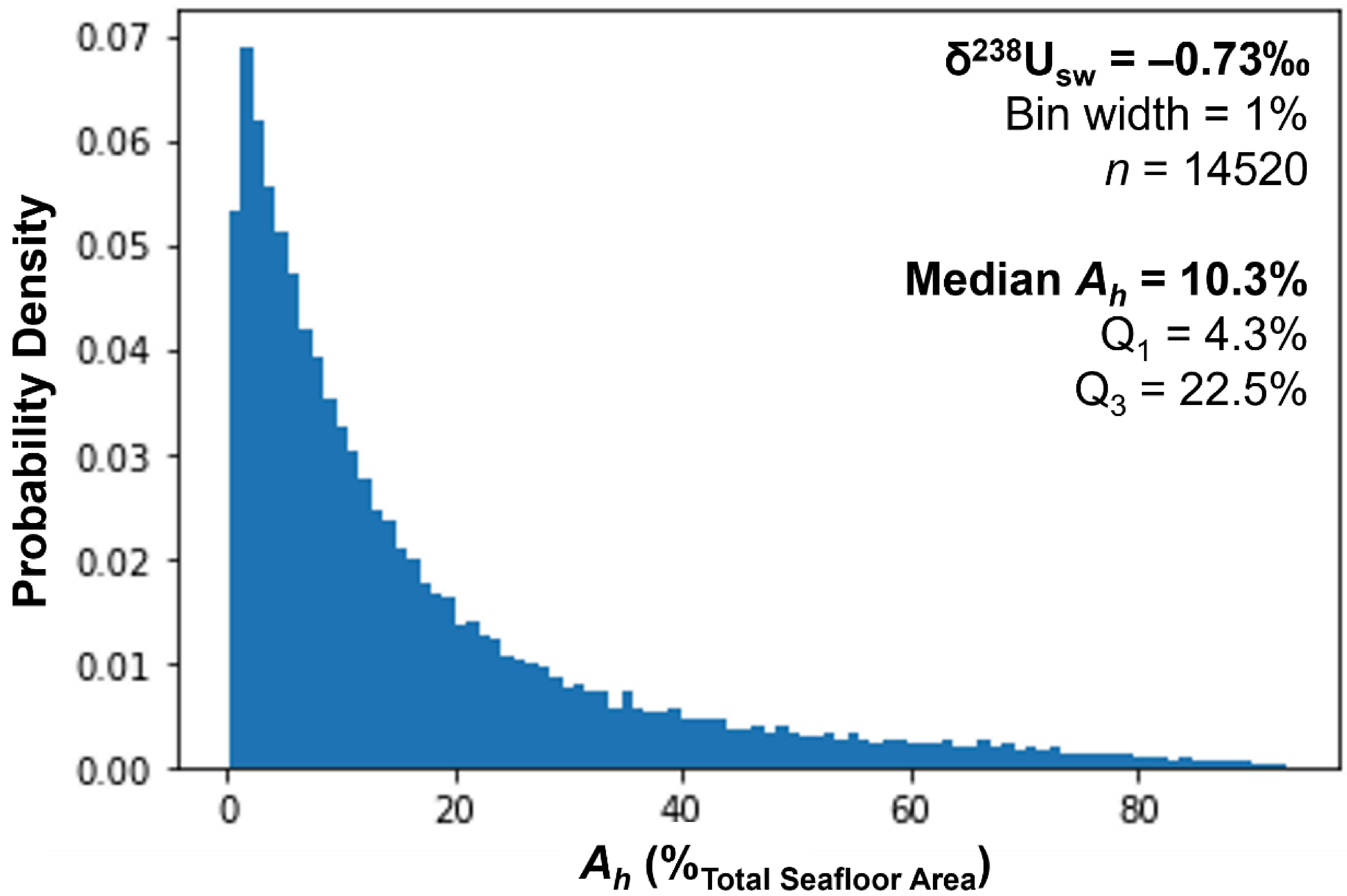

Figure S4. Results of U isotope mass balance model application (main text Equation 5) with $\delta^{238}U_{sw}$ set to minimum estimated Proterozoic $\delta^{238}U_{sw}$ (–0.73‰; Gilleaudeau et al., 2019) .

The model depicted in the block below can be used to estimate A_h through a range of $\delta^{238}U_{sw}$ as shown in the main text (i.e., from –0.73‰ to –0.29‰) with results in Figure S3.

```
import matplotlib as plt
import numpy as np

#Seawater range

d_sw_min = -0.73
d_sw_max = -0.29
d_sw_step = (d_sw_max-d_sw_min)/10

#Produce A_high histogram for selected seawater estimate range

Areas = []

for k_l in np.arange(0.048,0.5111,0.0421):
    for k_h in np.arange(0.469,2.7405,0.2065):
        for D_l in np.arange(-0.1,0.45,0.05):
            for D_h in np.arange(0.4,1.28,0.08):
                for d_sw in np.arange(d_sw_min,d_sw_max+d_sw_step,d_sw_step):
```

```
            A=A_high(k_l,k_h,D_l,D_h,d_sw)
            if 0<=A<=100:
              Areas.append(A)

plt.pyplot.hist(Areas,100,None,True)
print(np.percentile(Areas,(25,50,75)),len(Areas))
```

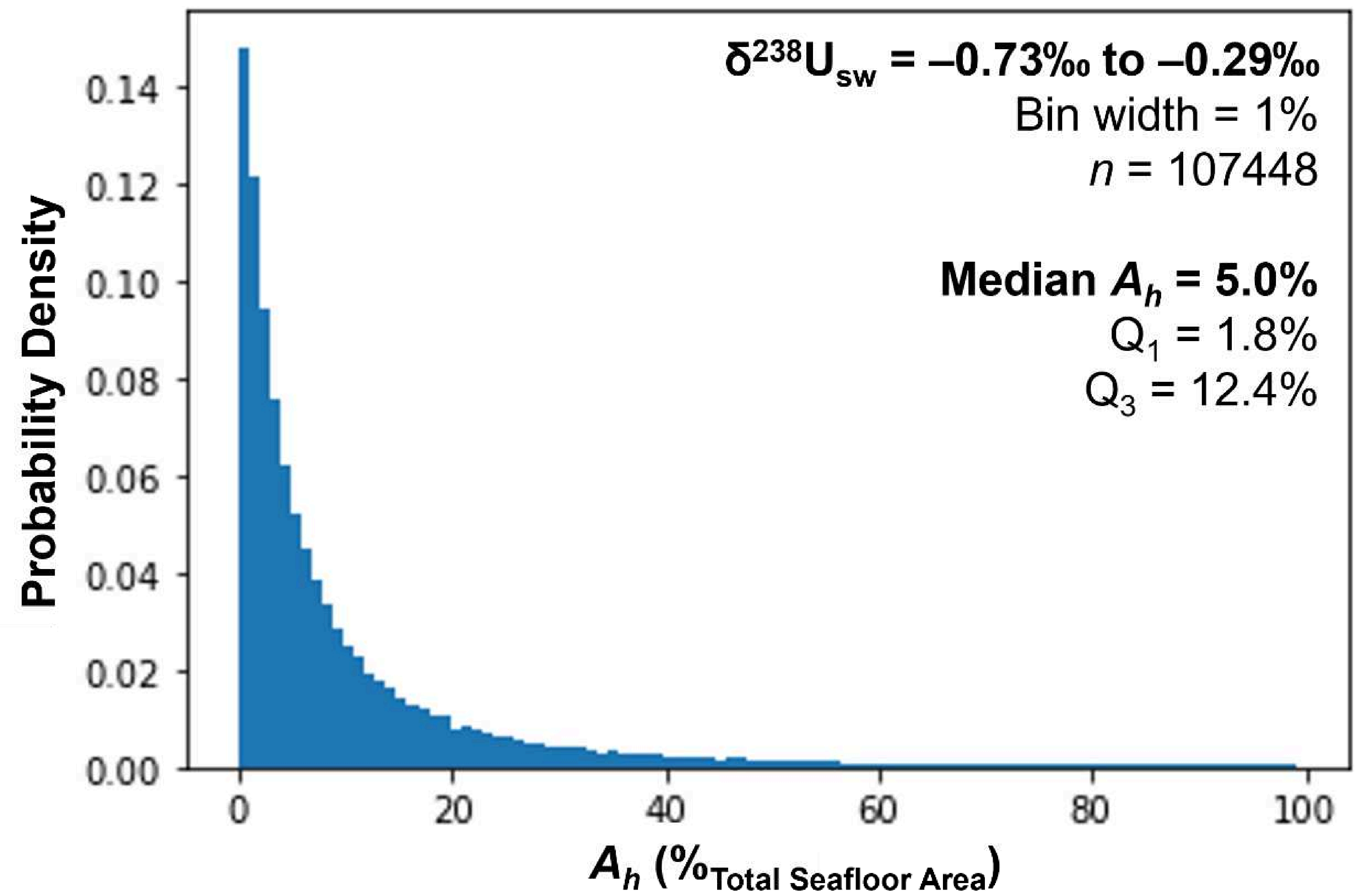

Figure S5. Results of U isotope mass balance model application (main text Equation 5) with variable $\delta^{238}U_{sw}$ from the estimated minimum Proterozoic seawater value (–0.73‰) to the modern $\delta^{238}U_{riv}$ (–0.29‰).

Supplementary References

Barovich, K.M., Patchett, P.J., Peterman, Z.E., Sims, P.K., 1989. Nd isotopes and the origin of 1.9-1.7 Ga Penokean continental crust of the Lake Superior region. GSA Bulletin 101, 333–338.

Bleeker, W., Kamo, S., Hamilton, M., Chamberlain, K., 2019. New age data and insights into the ca. 1887-1870 Ma Circum-Superior Belt, with startling implications for the Lake Superior area geology, in: Puumala, M. (Ed.), 65th Annual Meeting. Institute on Lake Superior Geology, Terrace Bay, ON, pp. 12–13.

Fralick, P.W., Davis, D.W., Kissin, S.A., 2002. The age of the Gunflint Formation, Ontario, Canada: single zircon U-Pb age determinations from reworked volcanic ash. Can J Earth Sci 39, 1085–1091. https://doi.org/https://doi.org/10.1139/e02-028

Gilleaudeau, G.J., Romaniello, S.J., Luo, G., Kaufman, A.J., Zhang, F., Klaebe, R.M., Kah, L.C., Azmy, K., Bartley, J.K., Zheng, W., Knoll, A.H., Anbar, A.D., 2019. Uranium isotope evidence for limited euxinia in mid-Proterozoic oceans. Earth Planet Sci Lett 521, 150–157. https://doi.org/10.1016/J.EPSL.2019.06.012

Hemming, S.R., McLennan, S.M., Hanson, G.N., 1995. Geochemical and Nd/Pb isotopic evidence for the provenance of the early Proterozoic Virginia Formation, Minnesota. Implications for the tectonic setting of the Animikie Basin. Journal of Geology 103, 147–168. https://doi.org/10.1086/629733

Hoffman, P.F., 1987. Early Proterozoic Foredeeps, Foredeep Magmatism, and Superior-Type Iron-Formations of the Canadian Shield, in: Kröner, A. (Ed.), Proterozoic Lithospheric Evolution. American Geophysical Union, pp. 85–98. https://doi.org/10.1029/GD017P0085

Holm, D., Boerboom, T.J., Scheiner, S., 2018. Reinterpretation of the ages of deposition and folding of Animikie Basin metasedimentary units in east-central Minnesota , in: Woodruff, L.G., Cannon, W.F., Stewart, E.K. (Eds.), Proceedings of the 64th Institute on Lake Superior Geology Annual Meeting. Institute on Lake Superior Geology, Iron Mountain, MI, pp. 51–52.

Holm, D., Cannon, W.F., Chandler, V.W., Schneider, D.A., Schulz, K., Van Schmus, W.R., 2005. The incredible shrinking Penokean Orogeny: a new look at the accretionary history of the southern Lake Superior region, in: Easton, M., Hollings, P. (Eds.), Proceedings of the 51st Institute on Lake Superior Geology Annual Meeting. Institute on Lake Superior Geology, Nipigon, ON, p. 27.

Johnston, D.T., Poulton, S.W., Fralick, P.W., Wing, B.A., Canfield, D.E., Farquhar, J., 2006. Evolution of the oceanic sulfur cycle at the end of the Paleoproterozoic. Geochim Cosmochim Acta 70, 5723–5739. https://doi.org/https://doi.org/10.1016/j.gca.2006.08.001

Klasner, J.S., Ojakangas, R.W., Schulz, K.J., Laberge, G.L., 1991. Nature and Style of Deformation in the Foreland of the Early Proterozoic Penokean Orogen, Northern Michigan, in: Sims, P.K., Carter, L.M.H. (Eds.), Contributions to Precambrian Geology of Lake Superior Region. U.S. Geological Survey, pp. K1–K22.

Larson, P., 2013. Chemostratigraphy of the Biwabik Iron Formation: Implications for Basin Longevity and Evolution, in: Blaske, A.R., Bornhorst, T.J. (Eds.), Proceedings of the 59th Institute on Lake Superior Geology Annual Meeting. Institute on Lake Superior Geology, Houghton, MI, pp. 50–51.

Maric, M., Fralick, P., 2005. Sedimentology of the Rove and Virginia Formations and their tectonic significance, in: Easton, M., Hollings, P. (Eds.), Proceedings of the 51st Institute on Lake Superior Geology Annual Meeting. Nipigon, Ontario, pp. 41–42.

Morey, G.B., 1969. The Geology of the Middle Precambrian Rove Formation in northeastern Minnesota. Minnesota Geological Survey, Minneapolis.

Morey, G.B., 1967. Stratigraphy and sedimentology of the Middle Precambrian Rove Formation in northeastern Minnesota. Journal of Sedimentary Research 37, 1154–1162. https://doi.org/10.1306/74D71857-2B21-11D7-8648000102C1865D

Morey, G.B., Southwick, D.L., 1995. Allostratigraphic relationships of early Proterozoic iron-formations in the Lake Superior region. Economic Geology 90, 1983–1993. https://doi.org/10.2113/GSECONGEO.90.7.1983

Ojakangas, R.W., Morey, G.B., Southwick, D.L., 2001. Paleoproterozoic basin development and sedimentation in the Lake Superior region, North America. Sediment Geol 141–142, 319–341. https://doi.org/https://doi.org/10.1016/S0037-0738(01)00081-1

Poulton, S.W., Fralick, P.W., Canfield, D.E., 2004. The transition to a sulphidic ocean ∼1.84 billion years ago. Nature 431, 173–177. https://doi.org/https://doi.org/10.1038/nature02912

Southwick, D.L., Morey, G.B., 1991. Tectonic Imbrication and Foredeep Development in the Penokean Orogen, East-Central Minnesota An Interpretation Based on Regional Geophysics and the Results of Test-Drilling, in: Sims, P.K., Carter, L.M.H. (Eds.), Contributions to Precambrian Geology of Lake Superior Region. U.S. Geological Survey, pp. C1–C17.

Van Wyck, N., Johnson, C.M., 1997. Common lead, Sm-Nd, and U-Pb constraints on petrogenesis, crustal architecture, and tectonic setting of the Penokean orogeny (Paleoproterozoic) in Wisconsin. GSA Bulletin 109, 799–808.